Liquid-vapor rectilinear diameter revisited

Y. Garrabos, C. Lecoutre, S. Marre, D. Beysens, and I. Hahn

Liquid-vapor rectilinear diameter revisited

Y. Garrabos[1,2], C. Lecoutre[1,2], S. Marre[1,2], D. Beysens[3], I. Hahn[4]

[1] *CNRS, ICMCB, UPR 9048, F-33600 Pessac, France*
[2] *Univ. Bordeaux, ICMCB, UPR 9048, F-33600 Pessac, France*
[3] *Laboratoire de Physique et Mï¿½canique des Milieux Hï¿½tï¿½rogï¿½nes,*
UMR CNRS-ESPCI ParisTech, Universitï¿½ Paris 6-7,
10 rue Vauquelin, F-75231 Paris Cedex 5, France and
[4] *Jet Propulsion Laboratory, California Institute of Technology, CA 91109, USA*
(Dated: 07 Dec 2017)

In the modern theory of critical phenomena, the liquid-vapor density diameter in simple fluids is generally expected to deviate from a rectilinear law approaching the critical point. However, by performing precise scanner-like optical measurements of the position of SF_6 liquid-vapor meniscus, in an approach much closer to criticality in temperature and density than earlier mesurements, no deviation from a rectilinear diameter can be detected. The observed meniscus position from far (10 K) to extremely close (1 mK) to the critical temperature is analyzed using recent theoretical models to predict the complete scaling consequences of a fluid asymmetry. The temperature dependence of the meniscus position appears consistent with the law of rectilinear diameter. The apparent absence of the critical hook in SF_6 therefore seemingly rules out the need for the pressure scaling field contribution in the complete scaling theoretical framework in this SF_6 analysis. More generally, this work suggests a new way to clarify the experimental ambiguities in the simple fluids for the near-critical singularities in the density diameter.

Phase transition is ubiquitous in nature. The most fecund phase transition is presumably through the liquid-vapor critical point accompanied by the spectacular critical opalescence, as already observed nearly two centuries ago. The vicinity of the critical points of many different systems is indeed characterized by strong singularities in their thermodynamic and transport properties. The current theoretical paradigm on critical phenomena, based on the use of renormalization group theory [1], has categorized all systems in well-defined universality classes [2] and characterized the singularities in terms of power-laws of only two relevant scaling fields [3] in a manner consistent with the scaling hypothesis [4]. Simple fluids are then assumed similar to the so-called $O(1)$ symmetric $(\Phi^2)^2$ field theory and (or) the $N = 1$-vector model of three-dimensional (3D) Ising-like systems [2, 5, 6]. However, for the case of the gas-liquid critical point of simple fluids, some additional difficulties can occur because the order parameter - the fluctuating local density - shows a noticeable asymmetry in the nonhomogeneous region, as for instance through the well-known rectilinear density diameter of the coexistence curve. The latter obeys the law $\rho_d = \frac{\rho_L + \rho_V}{2} = \rho_c + A_d (T_c - T)$ first evidenced by Cailletet and Mathias for three fluids [7]. ρ_L and ρ_V are the liquid and vapor densities of the coexisting phases and ρ_c is the critical density. T and T_c are the temperature and the critical temperature, respectively, and A_d is the experimental slope of the density diameter. Subsequent litterature has largely confirmed this law rectilinear diameter for a broad class of fluids (usually denoted normal fluids) with attemps to correlate the change of A_d with the differences in the two-body potential of molecular interaction [8, 9]. Nevertheless, such an asymmetrical linear form of the density diameter cannot be accounted

for from the symmetrical uniaxial 3D Ising model and its induced standard fluid-like version, i.e., the symmetrical lattice-gas model.

An alternate theoretical way to introduce the fluid asymmetry consists in mixing and extending the number of the physical fields contributing explicitly to the relevant scaling fields, so-called complete scaling phenomenological hypothesis [10–14]. The predictions of complete scaling have been tested against experiments with various fluid systems, especially binary solutions [15], and simulations representing ionic and polymer solutions with extraordinary asymmetry [12, 16]. In a recent work [17], Yang-Yang critical anomaly and singular density diameter arise in exactly soluble compressible cell gas models where complete scaling includes mixing with pressure field. However, the additional pressure field increases the complexity in the quest of a *true* asymptotic simple fluid behavior, which still remains a conundrum to the experimentalists who's objective is to check it experimentally closer and closer to the critical point. *De facto*, the asymmetrical contributions, the analytical backgrounds, and the classical-to-critical crossover corrections due to the mean-field-like critical point, further hindered the test of the asymptotic *Ising-like* fluid behavior. Such difficulties are intrinsically ineludible, even along the true critical paths where the crossover contribution due to one additional non-relevant field [18] can be accounted for correctly in the field theory framework [19–21].

All attempted experiments can never be strictly on these critical paths, adding paradoxically a new opportunity to investigate the theoretical expectations related to the non-symmetrical behaviors, as illustrated schematically in Fig. 1. Indeed, even though the temperature can be controlled very close to T_c in order to reach very small
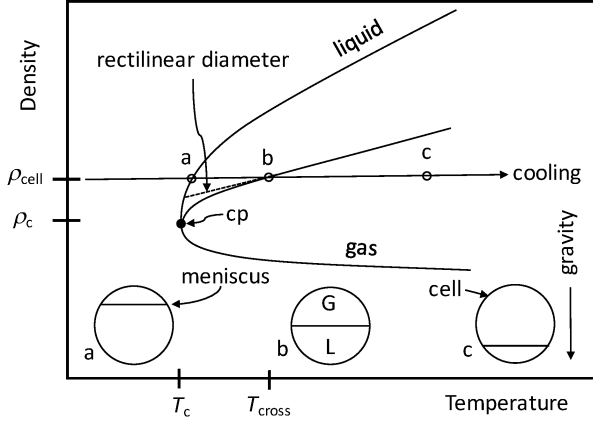
Figure 1: *Top*: Schematic diagram of coexisting liquid (upper branch) - gas (lower branch) density curve near the critical point (cp) of a simple fluid with critical temperature T_c and critical density ρ_c. Inside the two-phase domain, the *dashed* line and the *full* curve (with a "viewed hook" close to cp) correspond to the expected rectilinear and singular density diameters, respectively. The horizontal line at ρ_{cell} evidences three characteric points (**a,b,c**) along the thermodynamic path followed by cooling a cylindrical sample cell filled at a mean density $\langle\rho\rangle \equiv \rho_{cell}$ slightly above the critical density ($\langle\delta\tilde{\rho}\rangle = \frac{\langle\rho\rangle}{\rho_c} - 1 > 0$). *Bottom*: Expected meniscus positions of a two-phase cell during cooling: **a**: Above the volumetric median plane (VMP) of the cell at the coexistence temperature (very close to T_c); **b**: Matching the VMP of the cell at the temperature T_{cross} crossing the density diameter curve; **c**: Below the VMP of the cell far from T_c.

$\Delta\tau^* = \frac{T}{T_c} - 1$ values (lower than 10^{-5}, typically), the mean density $\langle\rho\rangle$ of the fluid cell of experiments has been hardly at its exact critical value ρ_c [22]. The error-bar related to the off-critical parameter $\langle\delta\tilde{\rho}\rangle = \frac{\langle\rho\rangle}{\rho_c} - 1$ never contribute to the discussion of the results in terms of true experimental distance to the critical point. Nevertheless, from the above experimental facts and the theoretical expectations, it appears that the related non-symmetrical effects can be investigated even in a slightly off-critical (liquid-like) density throughout the meniscus crossing the volumetric median plane (VMP) of the cell at a *single finite temperature distance* from T_c, i.e., $T_{cross} < T_c$, as shown in Fig. 1. From the symmetrical lattice-gas model, the meniscus of this liquid-like filled cell is expected to be visible always *above* this VMP in the two-phase temperature range.

Here, we intend to probe that SF$_6$, generally considered [23–25] as a standard simple fluid to support the critical asymmetry from complete scaling hypothesis [12–14], cannot exhibit the previously *viewed critical hook* (of 0.5% maximum amplitude) in the rectilinear density diameter close to the critical point, as schematically illustrated in Fig. 1. To support this examination, the relative uncertainty in the SF$_6$ filling density value was controlled within better than +/- 0.04% precision above 0.2% of the critical density, significantly lower than the

expected critical hook of 0.5% level.

The technical details of the test cell (called ALIR5 [26]) are given in the supplemental material (see also Ref. [27]). The viewed fluid volume consists in a quasi-perfect disk-shaped cylindrical fluid volume (of thickness $e_f = (2.510 \pm 0.002)$ mm and diameter $d_f = 2R = (10.600 \pm 0.005)$ mm). Its observation in light transmission leads to a two-phase fluid imaging similar to the schematic bottom views of Fig. 1. This viewed cylindrical fluid volume ($V_{fv} = \pi R^2 e_f = \left(221.50^{+0.20}_{-0.70}\right)$ mm^3 [28]) is surrounded by two opposite, small, and strictly similar dead volumes ($\frac{1}{2}V_{fb} = (7.1 \pm 0.2)$ mm^3), which correspond to the cell filling lines, positionned in the thickness median plane. This cell (of total fluid volume $V_f = V_{fv} + V_{fb} = \left(235.70^{+0.5}_{-1.0}\right)$ mm^3) was filled with 99.995% pure SF$_6$. The filling was made at a liquid-like mean density, such as $\langle\delta\tilde{\rho}\rangle = \frac{\langle\rho\rangle}{\rho_c} - 1 = \left(0.20^{+0.04}_{-0.04}\right)$ %, as measured from our filling and weighing processes. As schematically illustrated in the top part of Fig. 2, which shows the colored fluid cross sections for different directions of the VMP, 8 different cell configurations are used for the test. Each cell configuration is named (i, X), where the digit i represents two opposite gravity orientations (g↓ for $i = 1$ and g↑ for $i = 2$) and the letter X is associated with directions of the meniscus position and/or the VMP ($X = H$ for $\theta = 0°$, $X = V$ for $\theta = +90°$, $X = T$ for $\theta = +22.9°$ and $X = Z$ for $\theta = -23.2°$). We note that the (i, T) and (i, Z) configurations are not equivalent w.r.t. (*w.r.t.*) the liquid (or gas) positionning as, in the (i, T) case, one (on the gas-phase side) of the dead volumes can always act as a well for liquid trapping.

A similar temperature-timeline is used for each cell configuration during the temperature cooling of the cell, where temperature follows a log scale to cover the range 1 mK to 10 K from T_c. As discussed in the supplemental material, the exact value of T_c (highly reproducible over a 2 mK range from 318.721 K to 318.723 K for the 8 experimental runs) is not essential for the following analysis. The liquid-vapor meniscus is observed from optical transmission imaging through the cell, using LED illumination and cell view observation with a CCD camera (1024×1024 pixels) [29]. A physical pixel size corresponds to $12\,\mu$m. The image of each meniscus position data is recorded when thermal equilibration and density relaxation are achieved at each temperature distance $T_c - T$.

The highly symmetrical cell, the small off-critical average density filling, and the cell imaging provide highly-symmetrical behavior of the meniscus position as a function of temperature for both $(i = 1, 2, X)$ configurations *w.r.t.* gravity (see details in supplemental material). The exact position of the fluid in the cell image and the cell VMP are measured at sub-pixel level. The pixel coordinate of the meniscus, noted h_{iX}, is measured as one half part of the pixel difference between the bare positions, *i.e.*, by the distance from each VMP of the fluid cell. The temperature behavior of h_{iX} is reported in Fig. 2 for the 4 (i, X) directions. Except for the $(i, X = T)$ case
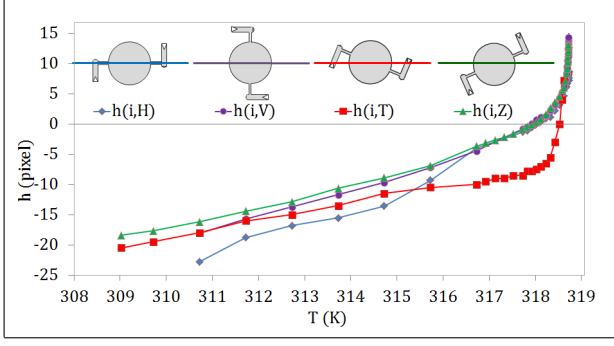
Figure 2: *(top)* Schematic cross-sectional orientation of the fluid volume and corresponding horizontal meniscus position close to its VMP. *(bottom)* Temperature dependence of both ($i = 1$ and $i = 2$) symmetrical pixel shifts of the meniscus position (w.r.t. each corresponding VMP), for the 8 (i, X) configurations. 1pixel=12μm.
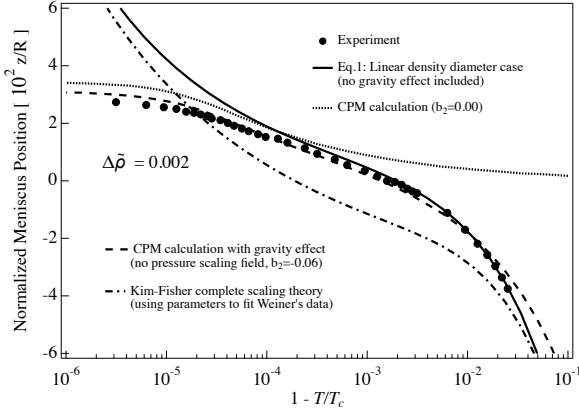

Figure 3: *Full circles:* Ratio $\frac{h}{R}$ for the (i, V) configuration, as a function of $1 - \frac{T}{T_c}$. *Full curve:* Eq. (1) with $\langle \delta \tilde{\rho} \rangle_{T_c} = 0.002$, using a $\Delta \tilde{\rho}_{LV}$ theoretical estimation without adjustable parameter (see text and Ref. [22] for details), $\tilde{\rho}_d = 1 + a_d \Delta \tau^*$ with $a_d = 0.84$, and capillary correction as defined in the text and supplemental material. *Dashed curve:* Normalized meniscus position $\frac{z}{R}$ obtained from CPM calculations for $\langle \delta \tilde{\rho} \rangle_{T_{coex}} = 0.002$, with compressible effects due to gravity (see text). *Dashed-dotted curve:* Eq. (1) for $\langle \delta \tilde{\rho} \rangle_{T_{coex}} = 0.002$ and $\Delta \tilde{\rho}_d$ given by Eqs. (3), using the the Kim and Fisher's [12] parameters.

discussed below, the temperature crossing of the VMP occurs in the range $317.823 \leq T_{cross} (\text{K}) \leq 318.123$ (accounting for ± 0.5-pixel uncertainty around $h_{iX} = 0$). Consequently, $T_c - T_{cross} \simeq (750 \pm 150)$ mK. Making reference to Fig. 1 and anticipating the following modelling approaches using non-dimensional quantities, we note that the knowledge of the corresponding reduced temperature distance $\Delta \tau^*_{cross} = \frac{T_{cross}}{T_c} - 1$ provides a single value of $\langle \delta \tilde{\rho} \rangle = \frac{\langle \rho \rangle}{\rho_c} - 1$. $\langle \delta \tilde{\rho} \rangle$ thus depends only on the related density diameter excess $\Delta \tilde{\rho}_d = \tilde{\rho}_d - 1$, (here $\tilde{\rho}_d = \frac{\rho_d}{\rho_c}$), without explicit knowledge of the absolute value of ρ_c.

The first modelling is based on the CPM model [30] of equation-of-state to define the temperature range where the gravity effects are significant. We use the mass conservation to derive a relationship between the average density and the local density profile of the compressible fluid. Modelling considers an ideal, non-dilatable cylindrical fluid sample volume of radius R and depth e_f, ignoring the role of the two dead volumes and neglecting the capillary effects. The CPM permits to estimate the local chemical potential (at position z) and the density profile $\rho(z)$ along the vertical axis of the cell. The density profile is a function of the temperature T, position z, and the CPM non-universal parameters $\bar{u}$, l_0, m_0, and b_2. The latter one, b_2, is often referred to as the field mixing parameter [31, 32], or asymmetry parameter since a well-defined value of b_2 appears characteristics of the singular asymmetry in the two-phase domain. Once we fix the constant average density of the cell, $\langle \rho \rangle = 1.002 \rho_c$ (*i.e.*, $\langle \delta \tilde{\rho} \rangle = 0.002$, see below), the corresponding meniscus position z_0 can be found through numerical integrations and root finding methods. Introducing a dimensionless variable $z^* = \frac{z}{R}$, the better fitting adjustment of z^* to $\frac{h_{iX}}{R}$ can be obtained for a particular set of the CPM parameters. Using our previous results $\bar{u} = 0.166$, $l_0 = 38.303$, $m_0 = 0.4877$ from fitting the SF_6 compressibility, heat capacity, and coexisting curves (see Ref. [22]) and fixing $b_2 = 0$ leads to the *dotted* curve in Fig. 3. This curve shows that the meniscus position can never be observed below the VMP of the cell. Such a behavior is also expected from the symmetrical uniaxial 3D-Ising model and the symmetrical lattice-gas model.

The modelling is thus performed by only using the parameter b_2 as a single adjustable quantity to explain the meniscus position behavior $\frac{h_{iX}}{R} (|\Delta \tau^*|)$ around T_{cross}. The result is illustrated by the *dashed* curve in Fig. 3, with $b_2 = -0.06 \pm 0.01$. Only the (i, V) configuration data are reported here to simplify the comparison with the experiments, especially approaching T_c where the contribution of the compressible effects does matter. Additional analytic modelling results obtained by changing the cell diameter from reference to $d_f = 2R$, have also confirmed that the relative importance of the effective cell height in the different configurations is significant only close to the critical temperature ($|\Delta \tau^*| < 10^{-4}$).

The results given in Fig. 3 support following remarks: (i) The compressibility effects become noticeable only within the reduced temperature range $|\Delta \tau^*| < 10^{-4}$, *i.e.*, $T_c - T \lesssim 30$ mK. We note that these effects can be observed in our experiment only in the temperature range $T_c - T \lesssim 15$ mK, using a grid shadow diagnosis [29] and/or local turbidity measurements on both sides of the gas-liquid meniscus; (ii) The CPM results (with $b_2 = -0.06 \pm 0.01$) shown as a *dashed* curve are consistent with the measured meniscus position around the crossing temperature of the VMP. Although the CPM calculation remarkably matches the current SF_6 data [6], we note that the value $b_2 = -0.06$ differs significantly from the value $b_2 = 0.035$ obtained using the direct description of

the Weiner's density diameter data in Ref. [24], even in its sign. Such results point out the practical difficulties to separate system-dependent parameters (*e.g.*, free amplitudes of the $|\Delta\tau^*|^{1-\alpha}$, $|\Delta\tau^*|$, and correction to scaling terms) unambiguously from the CPM modelling .

To shed light on this singular asymmetry problem, we used an additional modelling of the data, without reference to CPM, to analyze the meniscus behavior using a simple law of rectilinear diameter and compare it directly with the singular diameter case .

This second modelling can be performed in the temperature range $T_{\mathrm{coex}} - T > 30\,\mathrm{mK}$ where the gravity effects are neglected. A simple geometrical consideration (see Ref. [33]) based on the mass conservation inside the total volume, $V_f = V_{fv} + V_{fb} = \pi R^2 e_f \left(1 + x\right)$ (with $x = \frac{V_{fb}}{V_{fv}} \simeq 0.060$), leads to the following analytical form of $\frac{h}{R}$

$$\frac{h}{R} = \frac{\pi}{4} \frac{\langle\delta\tilde{\rho}\rangle_T - \Delta\tilde{\rho}_d}{\Delta\tilde{\rho}_{LV}} \left(1 + x\right) - \frac{\langle\delta h\rangle_{\mathrm{ca}}}{R}, \qquad (1)$$

The difference $\Delta\tilde{\rho}_d = \frac{\rho_L + \rho_V}{2\rho_c} - 1$ is the *excess* quantity from $\tilde{\rho}_d$, and $\Delta\tilde{\rho}_{LV} = \frac{\rho_L - \rho_V}{2\rho_c}$ is the *symmetrical* density coexistence curve. As detailed in supplemental material, two disturbing effects of the meniscus position are incorporated in Eq. (1) through the quantities $\langle\delta\tilde{\rho}\rangle_T$ and $\langle\delta h\rangle_{\mathrm{ca}}$, respectively. $\langle\delta\tilde{\rho}\rangle_T$ accounts for the cell thermal expansion through a linear approximation of the temperature change of the reduced average density change $\langle\delta\tilde{\rho}\rangle_{T_c}$ defined at T_c. The equivalent height $\langle\delta h\rangle_{\mathrm{ca}}$, assumed proportional to the squared capillary length, accounts for a practical approximation of the liquid volume involved in the capillary rise along the windows and the cell body. Here it is only essential to note that capillary rise effect can be neglected when $T_c - T \lesssim 3\,\mathrm{K}$, while the cell thermal expansion effect remains easy to estimate of 2 % at $T_c - T_{cross} \simeq 750\,\mathrm{mK}$ and lower than 8 % when $T_c - T < 3\,\mathrm{K}$. In such a latter temperature range only the first-term in Eq. (1) is thus important, and for $\langle\delta\tilde{\rho}\rangle_{T_c} > 0$, the meniscus crosses the median plane at T_{cross}, where $\langle\delta\tilde{\rho}\rangle_{T_{\mathrm{cross}}} = \Delta\tilde{\rho}_d$.

We first consider the rectilinear behavior of the reduced density diameter

$$\tilde{\rho}_d = 1 + a_d |\Delta\tau^*| \qquad (2)$$

where the excess quantity $\Delta\tilde{\rho}_d$ is proportional to $|\Delta\tau^*|$. The value $a_d = \frac{A_d T_c}{\rho_c} = 0.84 \pm 0.025$ is obtained analyzing the coexisting density data of Refs. [34, 35] on the two-phase temperature range $288\,\mathrm{K} \lesssim T \lesssim 316\,\mathrm{K}$. The measured value of T_{cross} corresponds to $\langle\delta\tilde{\rho}\rangle_{T_{\mathrm{cross}}} = (0.20 \pm 0.04)\%$. Accordingly, fixing $\langle\delta\tilde{\rho}\rangle_{T_c} = 0.002$ to calculate $\langle\delta\tilde{\rho}\rangle_T$, the *full* curve of Fig. 3 represents $\frac{h}{R}$ of Eq. (1), where $\Delta\tilde{\rho}_d = \tilde{\rho}_d - 1$ results from Eq. (2) and where is accounted for the capillary rise correction as given in supplemental material. The resolution in the image processing at the sub-pixel level is a key to the accurate determination of the filling density when the reduced slope

of the linear density diameter is only the *unknown* (but essential) physical parameter in the temperature range around T_{cross}. As shown in xenon [6] and similarly in Ref. [22] for SF_6, the singular top-shape of the reduced coexistence curve $\Delta\tilde{\rho}_{LV} \left(|\Delta\tau^*|\right)$ for $|\Delta\tau^*| \lesssim 10^{-2}$ was predicted without adjustable parameter, using the theoretical master crossover functions [21] estimated from the massive renormalization scheme [19, 20]. Nevertheless, any other effective power laws to describe $\Delta\tilde{\rho}_{LV}$ of SF_6 (such as $\Delta\tilde{\rho}_{LV} = 1.7147 |\Delta\tau^*|^{0.3271} + 0.8203 |\Delta\tau^*|^{0.8215} - 1.4396 |\Delta\tau^*|^{1.2989}$ from Ref. [25]) do not modify the current analysis, especially considering the two temperature decades $30\,\mathrm{mK} \leq T_c - T \leq 3\,\mathrm{K}$, where compressiblity and capillary rise effects are negligible.

We secondly consider the expected singular shape of the density diameter as predicted from the various complete field mixing approaches [10–14, 17]. The corresponding singular excess quantity presumably satisfies the following form:

$$\Delta\tilde{\rho}_d = \frac{A_\beta |\Delta\tau^*|^{2\beta} + A_\alpha |\Delta\tau^*|^{1-\alpha} + A_1 \Delta\tau^* + A_\Delta |\Delta\tau^*|^{x_\Delta}}{1 + a_\Delta |\Delta\tau^*|^\Delta} \quad (3)$$

with $\alpha = 0.109$, $\beta = 0.326$, $\Delta = 0.52$, and $x_\Delta = 1 - \alpha + \Delta$. Since 1974, several amplitude sets obtained from the Weiner's data fitting were published in literature [12, 14]. For clarity, only are here used in Eq. (3) the Kim and Fisher's [12] parameters, $A_\beta = 1.0864$, $A_\alpha = -7.990$, $A_1 = 9.770$, $A_\Delta = 0$, and $a_\Delta = 3.318$, noting no significant difference using any other literature parameter sets despite the large differences in the values of each amplitude term. By fixing $\langle\delta\tilde{\rho}\rangle_{T_c} = 0.002$, the corresponding estimation of $\frac{h}{R}$ is illustrated by the *dashed-dotted* curve in Fig. (3). Clearly, the $\frac{h}{R}$ calculations for the singular density diameter case are not compatible with our current experimental data, especially in the two decades $10^{-4} < |\Delta\tau^*| < 10^{-2}$, *i.e.*, $32\,\mathrm{mK} \lesssim T_c - T \lesssim 3.2\,\mathrm{K}$, where compressibility and capillary rising effects are negligible.

The noticeable inconsistency between the current data and any theoretical singular modelling based on Eq. (3) could be attributed to the fitting process of the $\tilde{\rho}_d$ experimental values using this non-analytic theoretical functional form. The main reason is presumably due to the large number of adjustable parameters in Eq. (3) and effective relative contributions of each power-law term at least one-decade larger than the maximum amplitude (0.5%) of the global excess deviation, especially close to the critical temperature. In addition, a systematic larger error-bar in these fitting results can be implicitly due to the Weiner's values of the critical parameters ρ_c, ε_c, and then $CM_c = \frac{1}{\rho_c} \frac{\varepsilon_c - 1}{\varepsilon_c + 2}$, which are significantly different (-1.35%, -10.9%, and -3.3%, respectively) from the litterature values [36].

As a conclusive remark, the predictive modelling of $\frac{h}{R}$ from Eq. (1) and rectilinear density diameter of Eq. (2) compare well (in amplitude and uncertainty) with

the measurements. Along the off-critical thermodynamic path of $(0.20 \pm 0.04)\,\%$ in the mean density, the high resolution imaging analysis of the SF_6 in two-phase domain shows no evidence of any singular hook-shapped deviation in the rectilinear density diameter near the critical point. The main part of the uncertainty in the rectilinear density diameter remains due to the accuracy (0.21%) for the SF_6 critical density value. In this simple experiment, the cell thermal expansion, the fluid compressibility, and the liquid wetting effects are well controlled, thanks to the highly symmetrical sample geometry, while the density diameter is understood without any additional adjustable parameters, except for the slope of the *linear* density diameter. More accurate data on SF_6 obtained in the new experiment is consistent with other normal fluids showing no detectable deviations from the rectilin-

ear diameter. Although the validity of the complete scaling theoretical framework has been well-demonstrated for many fluids systems including the binary solutions with extraordinary asymmetry, its experimental validation remains extremely challenging in one-component fluid systems.

[1] K. G. Wilson, Rev. Mod. Phys. **47,** 776 (1975).

[2] J. Zinn-Justin, *Quantum Field Theory and Critical Phenomena*, 4th ed. (Clarendon Press, Oxford, 2002).

[3] M. E. Fisher, J. Math. Phys. **5**, 944 (1964).

[4] H. E. Stanley, *Introduction to Phase transitions and Critical Phenomena* (Clarendon Press, Oxford, 1971).

[5] M. Barmatz, I. Hahn, J.A. Lipa, R.V. Duncan, Rev. Mod. Phys. **79**,1 (2007).

[6] Y. Garrabos, C. Lecoutre, S. Marre, D. Beysens, and I. Hahn, J. Stat. Phys. **158**, 1379-1412 (2015).

[7] L. Cailletet et E. Mathias, J. Phys. Theor. Appl., **5**, 1, 549-564 (1886).

[8] R. R. Singh and K. S. Pitzer, J. Chem. Physics **92**, 3096-3099 (1990).

[9] K. S. Pitzer and R. R. Singh, J. Chem. Physics **95**, 9426-9427 (1991).

[10] M. E. Fisher and G. Orkoulas, Phys. Rev. Lett. **85**, 696-699 (2000).

[11] Y. C. Kim, M. E. Fisher and G. Orkoulas, Phys. Rev. E **67**, 061506 (2003).

[12] Y. C. Kim and M. E. Fisher, Chem. Phys. Letters **414**, 185-192 (2005).

[13] M. A. Anisimov and J. Wang, Phys. Rev. Lett. **97**, 025703 (2006).

[14] J. Wang and M. A. Anisimov, Phys. Rev. E **75**, 051107 (2007).

[15] G. Pï¿½rez-Sï¿½nchez, P. Losada-Pï¿½rez, C. A. Cerdeirï¿½a, J. V. Sengers, and M. A. Anisimov, J. Chem Phys. **132**, 154502 (2010).

[16] See, e.g., M. E. Fisher, J. Stat. Phys. **75**, 1 (1994).

[17] C. A. Cerdeiriña, G. Orkoulas, and M. E. Fisher, Phys. Rev. Lett. **116**, 040601 (2016).

[18] F. J. Wegner, Phys. Rev. B **5**, 4529 (1972).

[19] C. Bagnuls and C. Bervillier, Phys. Rev. E **65**, 066132 (2002).

[20] Y. Garrabos and C. Bervillier, Phys. Rev. E **74**, 021113 (2006).

[21] Y. Garrabos, C. Lecoutre, F. Palencia, B. LeNeindre, and C. Erkey, Phys.Rev. E **77**, 021116 (2008).

[22] C. Lecoutre, R. Guillaument, S. Marre, Y. Garrabos, D. Beysens, and I. Hahn, Phys. Rev. E **91**, 060101(R) (2015).

[23] J. Weiner, K. H. Langley, and N. C. Ford Jr., Phys. Rev. Lett. **32**, 879 (1974).

[24] J. Weiner, Ph.D. thesis, University of Massachussetts, Amherst (1974).

[25] M. Ley-Koo and M. S. Green, Phys. Rev. A **16**, 2483-2487 (1977).

[26] ALIR5 test cell was selected among a series of 10 *identical* ALIRn cell (with $n = 1\,\text{to}\,10$). See also supplemental material.

[27] B. Zappoli, D. Beysens, and Y. Garrabos, *Heat Transfers and Related Effects in Supercritical Fluids* (Springer, Amsterdam, 2015), pp. 199-210.

[28] The negative error-bar includes an estimated fluid volume reduction of $0.5\,\text{mm}^3$ due to an internal glue volume excess resulting from the cell mounting process (see also Ref. [26]).

[29] see http://smsc.cnes.fr/DECLIC/index.htm

[30] V. A. Agayan, M. A. Anisimov, and J. V. Sengers, Phys. Rev. E **64**, 026125 (2001).

[31] J. V. Sengers and J. M. H. Levelt Sengers, Annu. Rev. Phys. Chem. 37, 189 (1986).

[32] N. D. Mermin and J. J. Rehr, Phys. Rev. Lett. 26, 1155 (1971).

[33] C. Morteau, M. Salzmann, Y. Garrabos, and D. Beysens, in *Proceedings of 2nd European Symposium Fluids in Space*, Ed. A. Viviani (Naples, 1996), pp. 327-333.

[34] R. Gilgen, R. Kleinrahm, and W. Wagner, J. Chem Thermodynamics **24**, 953 (1992).

[35] https://www.nist.gov/srd/refprop

[36] Weiner's values are $\rho_c = (0.731 \pm 0.001)\ \text{g\,cm}^{-3}$, $\varepsilon_c = 0.262^{+0.010}_{-0.009}$, and $CM_c = (0.1605 \pm 0.0001)\ \text{cm}^3\,\text{mole}^{-1}$. The most accurate litterature values are $\rho_c = (0.7420 \pm 0.0015)\ \text{g\,cm}^{-3}$, $\varepsilon_c = 0.2758 \pm 0.0018$, and $CM_c = (0.1657 \pm 0.0007)\ \text{cm}^3\,\text{mole}^{-1}$.